Band-Bending Effect in the Characterization of Subgap Density-of-States in Amorphous TFTs Through Fully Electrical Techniques

Heesung Lee, Jaewon Kim, Sungju Choi, Seong Kwang Kim, Junyeap Kim, Jaewon Park, Sung-Jin Choi, Dae Hwan Kim, and Dong Myong Kim

***Abstract*— We report a model for the band-bending effect (BBE) for improved extraction of the subgap density-of-states (DOS) in amorphous semiconductor thin-film transistors (TFTs). In previous works, the potential ($\psi(x)$) across the amorphous active layer was assumed to be the same as the surface potential (ψ_S) over the active layer without the BBE. Due to the distributed DOS ($g(E)$) over the bandgap and the modulation of the quasi-Fermi level ($E_F(x,V_{GS})$) by the gate bias, the non-uniform potential distribution should be considered in the characterization of DOS. We propose an empirical quadratic potential model ($\psi(x,V_{GS}) = \psi_S(V_{GS})(1 - x/t_{IGZO})^2$) for the BBE and extract a corrected distribution of DOS [$g(E)$]. We applied the BBE model to the amorphous indium–gallium–zinc oxide TFTs through the differential ideality factor technique. We extracted a corrected DOS as a superposition of two exponential functions with tail and deep state densities ($N_{To} = 8.8 \times 10^{17}$ eV^{-1}cm^{-3}, and $N_{Do} = 9 \times 10^{16}$ eV^{-1}cm^{-3}) at the tail and deep state characteristic energy ($kT_T = 18$ meV and $kT_D = 280$ meV), respectively. We confirmed the potential model and extracted DOS parameters by the TCAD simulation.**

***Index Terms*— Amorphous semiconductor, IGZO, Ideality factor, density-of-states, DOS, band bending, thin film transistor.**

I. Introduction

AMORPHOUS InGaZnO (a-IGZO) thin-film transistors (TFTs) are under active research and development for application in advanced display systems. a-IGZO channel is known to be advantageous over the carrier mobility, large area uniformity due to the amorphous phase, compatibility with the deposition process at low temperatures, and visible light transparency [1]–[3]. The electrical performance of amorphous semiconductors including multicomponent metal-oxides such as a-IGZO is determined by the atomic composition and the growing process [4]. Especially, the subgap density-of-states (DOS) distribution over the bandgap affect the operation and reliability of amorphous semiconductor TFTs. Therefore, accurate extraction of DOS over the bandgap in the amorphous film is one of the most important issues for characterization of degradation mechanisms and robust implementation of high performance display systems [5]. The distribution of DOS ($g(E)$ [cm^{-3}eV^{-1}]) near the conduction band minimum (E_C) is deterministic in the threshold voltage(V_T), the turn-on voltage (V_{ON}), the field effect mobility(μ_{FE}), the subthreshold slope (SS), and the on/off current ratio (I_{ON}/I_{OFF}).

Electrical extraction techniques of $g(E)$ in amorphous TFTs through the capacitance–voltage (C–V), current–voltage (I–V), and optical characteristics were reported [6]–[11]. However, the potential ($\psi(x)$) across the active layer is assumed to be the same as the surface potential ($\psi_S = \psi(x = 0)$) without considering the band bending effect (BBE). Therefore, the volume density of the DOS [eV^{-1}·cm^{-3}] is obtained from the experimental 2-dimensional DOS [eV^{-1}·cm^{-2}] simply divided by the active layer thickness (t_{IGZO} [cm]). Consequently, the extracted DOS without considering the BBE results in underestimated DOS due to the fixed assumption ($\psi(x) = \psi_S =$ constant) instead of the practically non-uniform distribution of the potential across the channel.

In this work, we propose a quadratic distribution of the potential ($\psi(x,V_{GS}) = \psi_S(V_{GS})(1 - x/t_{IGZO})^2$) for the BBE and extract a corrected DOS ($g(E)$) in amorphous TFTs. The BBE is combined with the differential ideality factor technique (DIFT [9]). We verified this proposed BBE model and the extracted result through the TCAD calculation of I-V characteristics in a-IGZO TFTs.

II. The Quadratic Potential Model for the Band Bending Effect in the Extraction of the DOS

We note that the energy band bending occurs across the active layer due to the gate bias and the quasi-Fermi level shifts from $E_F(x, V_{GS})$ to $E_F(x, V_{GS} + \Delta V_{GS})$ as schematically shown in Fig. 1(c)-(e). As a result, we observe a V_{GS}–dependent capacitance change ($\Delta C(V_{GS})$) in the C-V measurement caused by the cumulative charges from the distributed multiple DOS ($g(E)$) over the bandgap ($E \sim E + dE$) under subthreshold bias ($V_{FB} < V_{GS} < V_T$; $V_{FB} =$ the flat band, $V_T =$ the threshold voltage). We note that the capacitance change caused by the non-uniform distribution of the DOS appears in the ideality factor ($m(V_{GS})$) of the subthreshold I-V characteristics in amorphous TFTs.

Manuscript received November 30, 2016; accepted December 4, 2016. Date of publication December 7, 2016; date of current version January 24, 2017. This work was supported in part a National Research Foundation of Korea (NRF) Grant funded by the Korean Government (MSIP) (2016R1A5A1012966). The TCAD software was supported by Silvaco. The review of this letter was arranged by Editor A. Nathan.

H. Lee, J. Kim, S. Choi, S. K. Kim, J. Kim, S.-J. Choi, D. H. Kim, and D. M. Kim are with the School of Electrical Engineering, Kookmin University, Seoul 136-702, South Korea (e-mail: dmkim@kookmin.ac.kr).

J. Park is with the Department of Electrical and Electronic Engineering, South University of Science and Technology of China, Shenzhen 518055, China.

Color versions of one or more of the figures in this letter are available online at http://ieeexplore.ieee.org.

Digital Object Identifier 10.1109/LED.2016.2636301

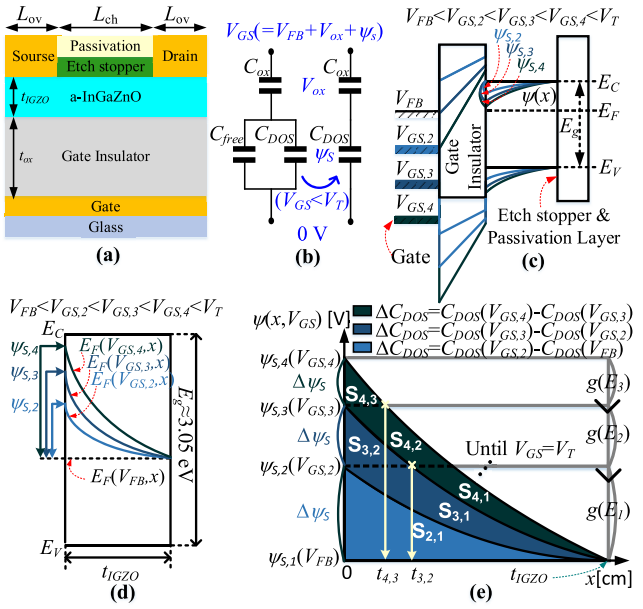

Fig. 1. (a) Bottom gate a-IGZO TFT structure. (b) Equivalent capacitance model for a-IGZO TFTs. (c) Energy band diagram in the subthreshold bias ($V_{FB} < V_{GS} < V_T$). (d) Potential distribution across the active layer. (e) Potential distribution for $V_{GS} > V_{FB}$. Each $_1C_{DOS}$ from the cumulative charges over the distributed multiple DOS ($g(E)$) below the quasi-Fermi level.

The drain current ($I_{D,SUB}$) under subthreshold bias is modeled to be

$$I_{D,SUB} \cong I_{Do} \exp\left(\frac{V_{GS}-V_T}{m V_{th}}\right) [\mathrm{A}]\,(V_{DS} > 3V_{th}) \tag{1}$$

$$I_{Do} = \mu_{eff} C_{ox} \left(\frac{W}{L}\right)(m-1)\, V_{th}^2\,[\mathrm{A}] \tag{2}$$

with m as the V_{GS}-dependent ideality factor, $V_{th}(= kT/\mathrm{q})$ as the thermal voltage, μ_{eff} as the effective electron mobility, $C_{ox}(= \varepsilon_{ox}/t_{ox})$ as the oxide capacitance per unit area, and W/L as the gate width/length ratio. As shown in the inset of Fig. 1(b), the channel capacitance, in a series with the oxide capacitance, consists of the free carrier-induced capacitance (C_{free}) and the DOS-induced capacitance (C_{DOS}) in parallel. In the subthreshold region, the DOS-induced capacitance (C_{DOS}) is greater than the free carrier-induced capacitance (C_{free}). Therefore, the V_{GS}-dependent ideality factor $m(V_{GS})$ can be approximated as

$$m\,(V_{GS}) = 1 + \frac{C_{free}+C_{DOS}}{C_{ox}} \cong 1 + \frac{C_{DOS}}{C_{ox}}. \tag{3}$$

From the experimental $I_{D,SUB} - V_{GS}$ data in Fig. 2(a), we obtain V_{GS}-dependent ideality factors and the differential ideality factor through

$$m\,(V_{GS}) = \left(\frac{\Delta V_{GS}}{V_{th}}\right) / \ln\left(\frac{I_{D,SUB}\,(V_{GS}+\Delta V_{GS})}{I_{D,SUB}\,(V_{GS})}\right) \tag{4}$$

$$\frac{dm\,(V_{GS})}{dV_{GS}} = \frac{1}{C_{ox}} \frac{dC_{DOS}\,(V_{GS})}{d\psi_S} \frac{d\psi_S}{dV_{GS}} \left[\mathrm{V}^{-1}\right]. \tag{5}$$

with ΔV_{GS} as the voltage step in the measurement and the surface potential ($\psi_S(V_{GS})$) as a non-linear function of the gate bias. The V_{GS}-dependent surface potential can be mapped from the C-V data through

$$\psi_S\,(V_{GS}) = \int_{V_{GS}=V_{FB}}^{V_{GS}} \left(1 - \frac{C_{G-DS}\,(V_{GS})}{C_{ox}\cdot W\cdot L}\right) dV_{GS}. \tag{6}$$

We finally obtain the DOS-induced $C_{DOS}(V_{GS})$ from the ideality factor through

$$C_{DOS}\,(V_{GS}) = \int_{\psi_S(V_{FB})}^{\psi_S(V_{GS})} C_{ox} \frac{dm\,(V_{GS})}{dV_{GS}} \left(\frac{d\psi_S}{dV_{GS}}\right)^{-1} d\psi_S \tag{7}$$

for a cumulative contribution of the DOS below the V_{GS}- dependent quasi-Fermi level ($E < E_F$) filled with electrons [9]. In the extraction of the DOS from $C_{DOS}(V_{GS})$, we assume that the DOS is spatially uniform across the active layer.

As shown in Fig. 1(e) under subthreshold bias, the potential distribution ($\psi(x, V_{GS})$) can be modeled empirically as a quadratic function of the location across the active layer as

$$\psi\,(x, V_{GS}) = \psi_{S,n}\left(1 - \frac{x}{t_{IGZO}}\right)^2; \quad n\text{=integer} \tag{8}$$

$$\psi_{S,n} \equiv \psi_S\left(V_{GS,n}\right) \tag{9}$$

$$V_{GS,n} = V_{FB} + (n-1)\,\Delta V_{GS}\,[\mathrm{V}]. \tag{10}$$

As shown in Fig. 1(e), ΔC_{DOS} counts the contribution of DOS ($g(E_n)$ [$\mathrm{eV}^{-1}\mathrm{cm}^{-3}$], n = integer) for the discrete energy level (E_n) and can be modeled as

$$\begin{aligned}\Delta C_{DOS}\left(\psi_{S,n}\right) &= C_{DOS}\left(\psi_{S,n+1}\right) - C_{DOS}\left(\psi_{S,n}\right) \\ &= q^2 \sum_{k=1}^{n} g\,(E_k) \frac{S_{n,k}}{\left(\psi_{S,k+1} - \psi_{S,k}\right)}\end{aligned} \tag{11}$$

with $g(E_k)$ as a DOS for the gate bias-modulated specific energy level(E_k) and the effective energy-depth area $S_{n,k}$[V·cm] as an integration over the bended active layer. Through Eq. (8), $S_{n,k}$ can be described as

$$S_{i,j} = \begin{cases} A\ (i = j+1) \\ A - \sum_{k=j+1}^{i-1} S_{i,k}\ (i \neq j+1) \end{cases} \tag{12}$$

$$\begin{aligned} A \equiv &\left(\int_0^{t_{i,j}} \psi_{S,i}\left(1 - \frac{x}{t_{IGZO}}\right)^2 dx - t_{i,j}\,\psi_{S,j}\right) \\ &- \left(\int_0^{t_{(i-1),j}} \psi_{S,i-1}\left(1 - \frac{x}{t_{IGZO}}\right)^2 dx - t_{(i-1),j}\,\psi_{S,j}\right) \end{aligned} \tag{13}$$

$$t_{i,j} = t_{IGZO}\left(1 - \sqrt{\frac{\psi_{S,j}}{\psi_{S,i}}}\right)\left(t_{i,1} = t_{IGZO}, t_{i,i}\,(= t_{j,j}) = 0\right) \tag{14}$$

with i and j as integers, and $t_{i,j}$ as the intersection of $\psi(x, V_{GS,i})$ and $\psi_{S,j}$. Finally, we extract $g(E_n)$ for each energy level from ΔC_{DOS} with the BBE from

$$g\,(E_n) = \left(\frac{C_{DOS}(\psi_{S,n+1}) - C_{DOS}(\psi_{S,n})}{q^2} - \sum_{k=1}^{n-1} g\,(E_k)\,\frac{S_{(n+1),k}}{\left(\psi_{S,k+1} - \psi_{S,k}\right)}\right) \Big/ \frac{S_{(n+1),n}}{\left(\psi_{S,n+1} - \psi_{S,n}\right)}. \tag{15}$$

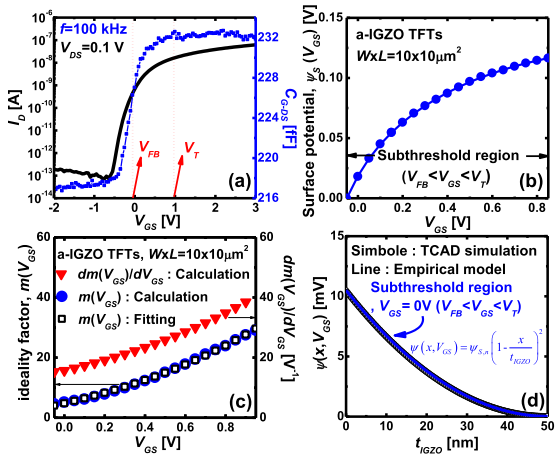

Fig. 2. (a) $I_D - V_{GS}$▷V_{DS} $\mathcal{D}$ 0.1 V) and $C_{G-DS} - V_{GS}$ characteristics ($f\,\mathcal{D}$ 100 kHz). (b) Surface potential (ψ_S▷V_{GS})) obtained from $C_{G-DS} - V_{GS}$ data through Eq. (6). (c) Ideality factor ($m(V_{GS})$) and differential ideality factor ($dm(V_{GS})/dV_{GS}$) obtained from $I_{D,SUB} - V_{GS}$ characteristics. (d) Empirical quadratic potential model for the potential distribution ψ▷x, V_{GS}◁ verified by TCAD simulation.

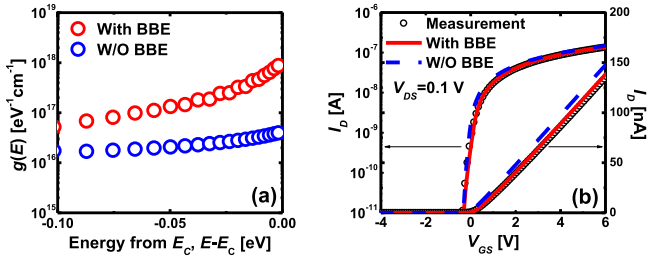

Fig. 3. (a) Extracted DOS with and without the BBE. (b) Measured data compared with the reproduced TCAD simulation with extracted DOS parameters.

III. Experimental Results and Discussion

For experimental verification of the quadratic BBE model for amorphous TFTs through a fully electrical technique, we adopt the DIFT for n-channel bottom gate a-IGZO TFTs with $W/L/L_{ov} = 10/10/6$ μm. The gate dielectric and active materials are SiO_x and a-IGZO with $t_{ox}/t_{IGZO} = 200/50$ nm as shown in Fig. 1(a). Measured $I_D - V_{GS}$ characteristics and the $C_{G-DS} - V_{GS}$ characteristics are shown in Fig. 2(a) for the employed a-IGZO TFTs. From the $C_{G-DS} - V_{GS}$ characteristics in the subthreshold region, as shown in Fig. 2(a), we obtained $V_{FB} = -0.2$ V at the maximum of dC_{G-DS}/dV_{GS}. A non-linear conversion of V_{GS} to ψ_S for the mapping of the energy level is shown in Fig. 2(b) with $m(V_{GS})$ in Fig. 2(c).

We obtained the threshold voltage V_T by the linear extrapolation in the $I_D - V_{GS}$ characteristics. As plotted in Fig. 2(c), the differential ideality factor $dm(V_{GS})/dV_{GS}$ is calculated from the fitted $m(V_{GS})$ based on the experimental data. Fig. 2(d) shows that the empirical quadratic model for the potential distribution $\psi(x, V_{GS})$ is well consistent with the TCAD simulation for the subthreshold operation.

As shown in Fig. 3(a) and TABLE I, the DOS $g(E)$ obtained from the DIFT considering the BBE is expressed as a superposition of the tail and deep states in exponential functions as

$$g(E) = N_{To} \cdot \exp\left(-\frac{E_C - E}{kT_T}\right) + N_{Do} \cdot \exp\left(-\frac{E_C - E}{kT_D}\right) \quad (16)$$

TABLE I
Extracted DOS Parameters With and Without the Band Bending Effect

$g(E)$	N_{To} [eV^{-1}cm^{-3}]	kT_T [eV]	N_{Do} [eV^{-1}cm^{-3}]	kT_D [eV]
W/O BBE	2.6×10^{16}	0.030	1.7×10^{16}	0.700
With BBE	8.8×10^{17}	0.018	9.0×10^{16}	0.280

where E_C as the conduction band minimum, kT_T and kT_D as the tail and deep state characteristic energy, N_{To} and N_{Do} as the characteristics tail and deep state characteristic density. We note that the characteristic energy (kT_T and kT_D) mainly governs the energy distribution or shape of the subgap DOS while the characteristic state density (N_{To} and N_{Do}) is determined by the composition of the metal oxides and fabrication process. Experimental result for the extracted DOS $g(E)$ with the BBE is comparatively shown in Fig. 3(a) and TABLE I. Without considering the BBE, ΔC_{DOS} is simply divided by t_{IGZO} even though the energy range below the quasi-Fermi level is not constant across the active layer. This underestimated DOS is corrected by considering the BBE in the extraction of $g(E)$ in this work. Obtained DOS with the BBE fully reproduces the $I_D - V_{GS}$ transfer characteristics as shown in Fig. 3(b). As shown in Fig. 3(a) and 3(b), the underestimated DOS without considering the BBE produces overestimated subthreshold swing (SS) and overestimated current in the above-threshold ($V_{GS} > V_T$) current. However, there is insignificant change in the turn-on voltage (V_{ON}: the marginal voltage for the drain current to sharply increase from the cut-off state to the subthreshold) whatever the BBE is considered or not. As observed in the result, tail state DOS parameters (N_{To} and kT_T) with a considerable difference by the BBE have a strong effect on SS and the above-threshold current. On the other hand, deep state DOS parameters (N_{Do} and kT_D) cause a considerable change in the turn-on voltage and a parallel shift of the transfer characteristics [5]. Therefore, in order to obtain accurate parameters (V_{on}, SS, and on-state driving current) for robust device design and consistent characterization of physical mechanisms in amorphous TFTs, the BBE should be fully considered in the characterization of the subgap DOS.

IV. Conclusion

Considering a cumulative contribution of the DOS below the V_{GS}-dependent quasi-Fermi level filled with electrons to the capacitance, we investigated the band bending effect in the characterization of the DOS in amorphous semiconductor TFTs. We proposed an empirical quadratic model for the potential across the amorphous active layer. Underestimated DOS is corrected by the V_{GS}-dependent band bending model and non-uniform potential distribution across the active layer. We confirmed the consistency of the quadratic potential model by TCAD simulation in a-IGZO TFTs. With the DOS parameters obtained from the DIFT with the BBE in a-IGZO TFTs, we fully reproduced I-V characteristics. We expect that the proposed BBE model and process is useful in the characterization of DOS in amorphous active layer through fully electrical C-V and I-V techniques for amorphous semiconductor TFTs.

REFERENCES

[1] J. H. Na, M. Kimura, and Y. Arakawa, "High field-effect mobility amorphous InGaZnO transistors with aluminum electrodes," *Appl. Phys. Lett.*, vol. 93, no. 6, p. 063501, Aug. 2008, doi: 10.1063/1.2969780.

[2] Y.-K. Moon, S. Lee, D.-H. Kim, D.-H. Lee, C.-O. Jeong, and J.-W. Park, "Application of DC magnetron sputtering to deposition of InGaZnO films for thin film transistor devices," *Jpn. J. Appl. Phys.*, vol. 48, no. 3, p. 031301, Mar. 2009, doi: 10.1143/JJAP.48.031301.

[3] E. Fortunato, P. Barquinha, and R. Martins, "Oxide semiconductor thin-film transistors: A review of recent advances," *Adv. Mater.*, vol. 24, no. 22, pp. 2945–2986, Jun. 2012, doi: 10.1002/adma.201103228.

[4] A. Olziersky, P. Barquinha, A. Vilà, C. Magaña, E. Fortunato, J. R. Morante, and R. Martins, "Role of Ga_2O_3–In_2O_3–ZnO channel composition on the electrical performance of thin-film transistors," *Mater. Chem. Phys.*, vol. 131, nos. 1–2, pp. 512–518, Dec. 2011, doi: 10.1016/j.matchemphys.2011.10.013.

[5] H.-H. Hsieh, T. Kamiya, K. Nomura, H. Hosono, and C.-C. Wu, "Modeling of amorphous InGaZnO_4 thin film transistors and their subgap density of states," *Appl. Phys. Lett.*, vol. 92, no. 13, p. 133503, Apr. 2008, doi: 10.1063/1.2857463.

[6] C. E. Kim, E. N. Cho, P. Moon, G. H. Kim, D. L. Kim, H. J. Kim, and I. Yun, "Density-of-states modeling of solution-processed InGaZnO thin-film transistors," *IEEE Electron Device Lett.*, vol. 31, no. 10, pp. 1131–1133, Oct. 2010, doi: 10.1109/LED.2010. 2061832.

[7] S. Lee, S. Park, S. Kim, Y. Jeon, K. Jeon, J. H. Park, J. Park, I. Song, C. J. Kim, Y. Park, D. M. Kim, and D. H. Kim, "Extraction of subgap density of states in amorphous InGaZnO thin-film transistors by using multifrequency capacitance–voltage characteristics," *IEEE Electron Device Lett.*, vol. 31, no. 3, pp. 231–233, Mar. 2010, doi: 10.1109/LED.2009.2039634.

[8] H. Bae, H. Seo, S. Jun, H. Choi, J. Ahn, J. Hwang, J. Lee, S. Oh, J.-U. Bae, S.-J. Choi, D. H. Kim, and D. M. Kim, "Fully current-based sub-bandgap optoelectronic differential ideality factor technique and extraction of subgap DOS in amorphous semiconductor TFTs," *IEEE Trans. Electron Devices*, vol. 61, no. 10, pp. 3566–3569, Oct. 2014, doi: 10.1109/TED.2014.2348592.

[9] M. Bae, D. Yun, Y. Kim, D. Kong, H. K. Jeong, W. Kim, J. Kim, I. Hur, D. H. Kim, and D. M. Kim, "Differential ideality factor technique for extraction of subgap density of states in amorphous InGaZnO thin-film transistors," *IEEE Electron Device Lett.*, vol. 33, no. 3, pp. 399–401, Mar. 2012. doi: 10.1109/LED.2011.2182602

[10] M. Dai, K. Khan, S. Zhang, K. Jiang, X. Zhang, W. Wang, L. Liang, H. Cao, P. Wang, P. Wang, L. Miao, H. Qin, J. Jiang, L. Xue, and J. Chu, "A direct method to extract transient sub-gap density of state (DOS) based on dual gate pulse spectroscopy," *Sci. Rep.*, vol. 6, p. 24096, Jun. 2016, doi: 10.1038/srep24096.

[11] E. K.-H. Yu, S. Jun, D. H. Kim, and J. Kanicki, "Density of states of amorphous In-Ga-Zn-O from electrical and optical characterization," *J. Appl. Phys.*, vol. 116, no. 15, p. 154505, 2014.